

The “DNA” of chemistry: Scalable quantum machine learning with “amons”

Bing Huang and O. Anatole von Lilienfeld*

*Institute of Physical Chemistry and National Center for Computational Design and Discovery of Novel Materials (MARVEL),
Department of Chemistry, University of Basel, Klingelbergstrasse 80, 4056 Basel, Switzerland*

(Dated: November 24, 2021)

Given sufficient examples, recently introduced machine learning models enable rapid, yet accurate, predictions of properties of new molecules. Extrapolation to larger molecules with differing composition is prohibitive due to all the specific chemistries which would be required for training. We address this problem by exploiting redundancies due to chemical similarity of repeating building blocks each represented by an effective atom in molecule: The “am-on”. In analogy to the DNA sequence in a gene encoding its function, constituting amons encode a query molecule’s properties. The use of amons affords highly accurate machine learning predictions of quantum properties of arbitrary query molecules in real time. We investigate this approach for predicting energies of various covalently and non-covalently bonded systems. After training on the few amons detected, very low prediction errors can be reached, on par with experimental uncertainty. Systems studied include two dozen large biomolecules, eleven thousand medium sized organic molecules, large common polymers, water clusters, doped *h*BN sheets, bulk silicon, and Watson-Crick DNA base pairs. Conceptually, the amons extend Mendeleev’s table to account for the chemical environments of elements. They represent an important stepping stone to machine learning based virtual chemical space exploration campaigns.

The basic concept of fundamental building blocks, determining the behaviour of matter through their specific combinations, has had a profound impact on our understanding of particle physics (quarks) [1], electronic structure of atoms and molecules (elemental particles) [2], or proteins and genetic codes (amino and nuclear acids) [3]. Within the molecular sciences, the transferability among functional groups has enabled synthetic chemists to reach remarkably precise control over intricate complex atomistic processes. Theoretical chemistry has yet to transform such chemical intuition into an equally efficient and transferable approach. If universally predictive this would manifest a profound understanding of chemistry, and enable the computational exploration of chemical space [4] with unprecedented scale and precision. Important molecular and materials design challenges could then be tackled, possibly alleviating many of today’s pressing problems due to lack of new drugs, clean water, or efficient catalysts.

Unfortunately, reliable and generic virtual exploration campaigns in chemical space remain prohibitive due to the considerable computational cost of state-of-the-art quantum methods, such as density functional theory (DFT) [5, 6]. Within the last decade, novel machine learning (ML) models have introduced alternative ways to efficiently tackle long-standing fundamental problems in physics and chemistry [7–20]. The transferability required to screen chemical compounds of larger size and diverse composition, however, has not yet been reached by these ML models. Various *ab initio* strategies have already been proposed to address scalability [21–27]. Unfortunately, these methods typically either trade predictive transferability for speed, or continue to suffer from steep scaling pre-factors. We tackle this outstanding challenge by combining the ideas of training set selec-

tion with a new ML representation and quantum chemistry reference numbers. Since fragments repeat throughout chemical space, independent of the specific query molecule at hand, they can be viewed as indistinguishable entities each corresponding to an atom in molecule, dubbed “am-on”. In close analogy to DNA sequences encoding the functionality of genes, sets of amons can be used to infer properties of molecules. Explicitly accounting for all the possible chemical environments of each element, amons effectively extend the dimensionality of Mendeleev’s table, as illustrated in Figure 1. To demonstrate the versatility of this idea, we present results for amon based ML predictions applied to a multitude of systems, including two dozen large biomolecules, eleven thousands of medium sized organic molecules, five common polymers, and six water clusters with up to 21 molecules, three doped *h*BN sheets, bulk silicon, and Watson-Crick bonded DNA base pairs. We are not aware of any alternative approach which provides similar convergence behaviour and extrapolative capabilities.

When breaking up large query molecules, e.g. through cascades of bond separating reactions, [28] increasingly smaller and more common molecular fragments are obtained, whose summed up energy will increasingly deviate from query. To control the errors resulting from our *Ansatz*, we perform the reverse procedure: Starting very small, increasingly larger amons (representing fragments) are being included in training, resulting in increasingly more accurate ML models. The training set size is minimized by selecting only the most relevant amons, i.e. those small fragments which retain the same local chemical environment as encoded through the coordinates of the query molecule, obtained through preceding DFT relaxation. Note that query coordinates resulting from less expensive force-field methods, such as [29],

could have been used just as well [30].

Figure 2 illustrates the amon ML (AML) approach for predicting the total potential energy of the organic molecule 2-(furan-2-yl)propanol ($C_7H_{10}O_2$): The AML prediction improves systematically as more and larger amons are being included in the training, being selected through the subgraph matching algorithm, and reaching ~ 1.5 kcal/mol prediction error with no more than 31 amons with at most 6 heavy atoms each. To exceed chemical accuracy (~ 1 kcal/mol prediction error) the training set requires inclusion of 7 additional amons with 7 heavy atoms each. By comparison, tens of thousands of training molecules are needed to reach similar prediction errors using conventional ML models trained on randomly selected molecules [10, 20]. Inspection of the selected amons reveals that all “local chemistries”, present in the molecule, have been dialled in. For example, alcohols with respectively sp^3 - and sp^2 -hybridized carbon atoms in vicinal and geminal position to the hydroxy group are present among all amons with more than three heavy atoms. While the prediction error in Figure 2D decreases systematically with amon and training set size, the sign indicates that the query energy is underestimated by AML for smaller amons with up to 3 heavy atoms (lack of stabilization through electronic delocalization), and overestimated for larger amons with more than 4 heavy atoms (overly stabilized due to unconstrained conjugated double bonds). Note that due to the oscillatory nature of the convergent prediction error, it is possible to prematurely reach spuriously low errors for unreasonably small amons by mere coincidence. For example, for 2-(furan-2-yl)propanol an error of only ~ 10 kcal/mol can be found using only 9 amons with no more than 3 heavy atoms. It is therefore important to systematically converge AML prediction errors. Figure 2D also illustrates that AML models of other size-extensive properties can trivially be generated using the exact same kernels as for energies: The prediction error for the isotropic static molecular polarizability is shown as well, and it reaches ~ 0.4 Bohr³, on par with hybrid DFT accuracy [31].

Note that in comparison to more conventional homodermotic construction approaches [27, 32] (see also references therein) our AML model differs by (a) the amon selection algorithm which automatically solves the problem of how to partition the system into its constituting fragments, (b) the specific linear combination of energy contributions, appropriately weighted through use of kernel ridge regression, (c) the averaging out of combinatorially many fragmentation schemes which represent the buffer regions linking different amons, and (d) the broader applicability to non-covalent binding and condensed phase.

To make use of an efficient AML implementation, we developed a two and three-body interatomic potential based representation of atoms in molecules. Due to its popularity we have used hybrid DFT (B3LYP) for train-

ing and validation throughout. We note that the choice of reference is irrelevant for AML, any other level of theory could have been used just as well. To corroborate this fact, we have calculated Hartree-Fock, MP2, and CCSD(T) reference based AML learning curves for water clusters. More specifics and computational details are given below and in Supplementary Materials.

The prediction of total energies for two dozen large and important biomolecules, including cholesterol, cocaine, taxol, or NADH can be considered to illustrate the scalability and usefulness of AML in the most compelling fashion. True versus predicted energies are shown in Figure 3 for various AML models trained on sets of amons containing $N_I = 1, 2, 3, 5,$ and 7 heavy atoms. Systematic improvement of predictive accuracy is found reaching mean absolute errors typically associated with bond-counting, density functional theory, or experimental thermochemistry for amons with 3, 5, or 7 heavy atoms, respectively. For smaller query molecules with rigid and strain-less structure and homogeneous chemical environments of the constituting atoms, e.g., vitamin B3 with only 9 heavy atoms, the prediction error decreases faster with amon size than for more complex molecules, reaching chemical accuracy with less than one hundred amons in total (see supplementary materials for detail). Not surprisingly, large and complex molecules with diverse atomic chemical environments, such as NADH, require substantially more amons to reach the same level of accuracy. On the scale of atomization energies, the results also reflect basic chemistry: Predicted energies decrease towards the reference as the amons account for contributions corresponding to composition ($N_I = 1$), bonds ($N_I = 2$), and hybridization ($N_I = 3$).

When exploring chemical space one invariably faces the problem of severe selection bias due to the unfathomably large scale resulting from all the possible combinations of atom types and coordinates. In order to rule out the possibility of above results being coincidental, we have investigated the AML performance for eleven thousand diverse organic query molecules made up of nine heavy atoms. All query molecules were drawn at random from the QM9 dataset [33, 34] consisting of coordinates and electronic properties of 134k organic molecules calculated at the hybrid DFT level of theory. While QM9 certainly constitutes by no means a comprehensive subset of chemical space [4, 35], it is representative for substantial branches of chemistry. Furthermore, conclusions regarding AML are drawn without loss of generality: Any other molecular data set could have been chosen just as well.

After amon selection and subsequent training, out-of-sample prediction errors of atomization energies decrease systematically with number and size of amons (See Figure 4A), and reach 1.6 kcal/mol for amons with up to seven heavy atoms. Corresponding standard deviations tend to be independent of training set size. Note that such training set sizes are two to three orders of mag-

nitude smaller than for conventional neural network or kernel ridge regression models which rely on random sampling and which do not scale [18, 20]. Examining molecules one by one, we find that largest deviations correspond to molecules containing highly strained fragments, example shown in Figure 4A. In order to properly account for strained query molecules, the training set would require inclusion of amons with similarly strained local motifs.

Application of the amon selection algorithm to the 110k organic molecules in QM9 with nine heavy atoms results in a grand total of only ~ 21 k amons with up to seven heavy atoms (all specified in the Supplementary Material). While distinct, these ~ 21 k amons are indistinguishable in the sense that they do not depend on any possible query molecule, but can rather be combined to model arbitrarily many new and different query molecules with an expected MAE in atomization energy of ~ 1.6 kcal/mol. The exponentially decaying normalized frequency distribution of amons with number of atoms is shown in Figure 4B, along with the exponentially growing number of possible molecules in QM9. As one would expect, the smaller the amon the more frequently it will be selected, and for any given amon size high carbon content is more frequent than high oxygen or nitrogen content. A list and a movie, displaying the one thousand most frequent amons are provided in the supplementary materials. Conversely, the larger the amon the less likely that it will be needed for predicting properties of a random query molecule. It is hence consistent that the ten least frequent amons, not shared by any pair of query molecules, represent rather pronounced chemical specificity (shown in Figure 4B). These results amount to numerical evidence that the fundamental idea of using amon based building blocks within ML models is meaningful for chemistry: The larger the query molecule and the weaker the accuracy requirements, the more query molecules will share the same amons. As such, the AML model effectively exploits the lower dimensionality of fragments in the very high dimensional chemical space, known to scale exponentially with number of atoms [33, 35].

The use of AML can deepen our understanding of chemistry. E. g. consider the number and nature of amons shared among different query molecules. They can serve as an intuitive measure of chemical similarity, as exemplified for three organic query molecules in Figure 4C. The smallest amons are shared by all molecules, and the more similar a pair of query molecules the larger the “genetic” overlap: Molecules I and II are more similar than I and III, which are more similar than II and III. Shared amons imply that AML predictions of other compounds will require fewer additional reference data. Another valuable insight obtained from AML is the transferability of regressed atomic energies: Local atoms possessing similar environments will contribute to similar de-

grees to the total energy, which also underpins the atoms-in-molecules theory [36]. To illustrate this, atomic contributions to the AML estimated atomization energies are also printed for the three example molecules in Figure 4C (see Supplementary Material for more detail). Note that their relative values are consistent with chemical intuition about covalent bonding. For example, there are three types of local oxygen environments (carbonyl, alcohol, and furane) which contribute to covalent binding (~ 94 , 94, and 100 kcal/mol, respectively) in an order which one would expect for an atom sharing one double bond to carbon, two single bonds (carbon, hydrogen), and being in a conjugated environment (furane). Also, sp^3 -hybridized, aromatic, and sp^2 -hybridized (in carbonyl) carbon atoms contribute with ~ 164 , ~ 162 , and 157 kcal/mol, respectively, also reflecting the fact that four single bonds contribute more bonding energy than two single and one double bond, and that aromaticity provides additional stabilization. It is also consistent that hydrogen atoms have a relatively small variance in their contribution (64 to 66 kcal/mol), they can only have single bonds. For comparison, we have also calculated corresponding energies using reparameterized Morse potentials [37]. Overall fair agreement with corresponding Morse numbers is found, suggesting the capability of AML to provide qualitative and quantitative insight to a degree previously only accessible through physically motivated approximations. Note that, obviously, Morse potential based estimates of atomization energies of such molecules are dramatically worse than AML due to their averaged parameters, rigid functional form, and inherent neglect of interatomic many-body effects.

After showcasing AML results for thousands of organic molecules we now focus on the question of scalability. While some of the biomolecules in Figure 3 are already substantially larger than the amons employed with no more than seven heavy atoms, we have investigated the applicability of AML to very large systems in a more systematic fashion. Four different classes of systems, somewhat representative for the chemical space spanned by early main group elements, have been examined; and we have found that regardless of size and chemical nature, all prediction errors decrease systematically and reach rapidly chemical accuracy as number and size of selected amons grows: (i) We have trained AML models to predict total potential energies of five common polymers with increasing size and chemical complexity (polyethylene ($N_I = 26$), polyacetylene ($N_I = 30$), alanine peptide ($N_I = 50$), polylactic acid ($N_I = 50$) and the backbone of quaternary ammonium polysulphone ($N_I = 96$)). The latter being essential for alkaline polymer electrolyte fuel cells) [38]. Resulting learning curves in Figure 5A exhibit a simple trend: The more chemically complex the system, the more amons are selected and required in order to achieve predictive power. The chemically most complex polymer polysulphone requires nearly ten times more

amons (~ 200) to reach chemical accuracy (~ 1 kcal/mol), than polyethylene, the chemically simplest polymer in our set (~ 20). (ii) Potential energies of water clusters consisting of eleven, thirteen, fifteen, seventeen, nineteen and twentyone [39] molecules have been predicted (see Figure 5B). Also in this case, prediction errors decay rapidly and systematically for all clusters and reach chemical accuracy with at most seven amons and no more than ten water molecules/amons. This demonstrates the applicability of AML to non-covalent hydrogen-bonding. (iii) We have examined periodic 2D materials, namely hexagonal BN sheets doped with carbon and gold (C-*h*BN; Au-*h*BN; C,Au-*h*BN), previously reported to have very high efficiency towards CO oxidation reaction [40] (see Figure 5C). Due to substantial redundancy caused by underlying symmetries, AML prediction errors of total energies converge to chemical accuracy within at most twelve amons for the most complex C,Au-*h*BN doped variant. (iv) Symmetry plays an even more important role in crystalline bulk: To accurately predict the cohesive energy of silicon only five amons with no more than eighteen atoms are required (see Figure 5D). Interestingly, a AML lattice scan produces even a reasonable minimum—despite the lack of distorted amons for training. We believe that this is due to the aforementioned fact that the AML model approaches the energy from above.

It is a hallmark of machine learning models that in the limit of large training set size N they systematically improve with N . Logarithmized prediction errors of kernel ridge regression models decay linearly with logarithmized training set size [41], as long as training data and molecular representations are noise-free and unique, respectively [37]. All AML learning curves obtained so far confirm that off-set and slope improve dramatically in comparison to learning curves of conventional ML models which do not scale and rely on random sampling of training molecules [10, 20, 37]. We believe that the AML’s advantageous performance results from (i) a scalable building block approach, physically motivated by the observation that effective atoms can be transferable in molecules [36], ultimately reducing the formal dimensionality of the potential energy hyper surface in chemical space [35]. Dimensionality reductions are known to lead to steeper learning curves [42]. (ii) a compact and minimalistic representation (SLATM), based on interatomic many-body terms, which meets crucial criteria identified in Ref. [37], and which also lowers the learning curve off-sets (see Supplementary Materials for more details). (iii) elimination of counterproductive or redundant training species through subgraph matching, which amounts to an optimization of training set composition, already shown to lead to substantial reduction in learning-curve off-set after application of genetic algorithms [43]. Note that in the limit of small training set N , prediction errors do not necessarily decay in a monotonic fashion with N .

However, our selection procedure focusses on the most relevant training instances, and thereby filters out those cases which could potentially deteriorate the prediction. Consequently, steeper slopes of AML learning curves with improved monotonicity are found, even for small N .

Finally and out of curiosity, we have investigated the “DNA” of DNA, i.e. the amons of DNA. More specifically, we have considered the Watson-Crick Cytosine-Guanine (GC) base pair (see Figure 6E). While amons with no more than seven heavy atoms suffice to converge the energies for individual base pairs, amons corresponding to truncated motifs of hydrogen bonds with up to ten heavy atoms are necessary to reach chemical accuracy. Similar performance has been observed for the Watson-Crick bonded Adenine-Thymine base pair (See supplementary materials). It is not surprising that non-covalent bonding patterns, such as Watson-Crick bonding, require larger amons, as they extend over larger spatial domains. Furthermore, they also exhibit strong non-local effects through their conjugated moieties, implying the need for amons with multiple hydrogen bonds. Interestingly, to reach chemical accuracy it is not necessary to include amons which simultaneously contain aromatic fragments and hydrogen bonds, justifying previously made system choices for the study of nuclear quantum effects in DNA [44].

We have combined the idea of building blocks in chemistry (amons) with machine learning to rapidly and systematically infer quantum properties of large and arbitrary query molecules. Seen the strong transferability and versatility of AML, predicting a query molecule’s properties based on its constituting amons, there is a strong analogy to DNA sequences which also encode the functionality of genes. Another analogy can be drawn with respect to linguistics. The list of possible amons could represent a “dictionary” of chemistry, and molecules and their properties would correspond to sentences and their meaning. Zipf’s law, however, does not appear to be applicable in the case of amons. More rigorously, we think of amons as an additional dimension in the periodic table (Fig. 1) which accounts for chemical environment. Due to well defined similarity measures, any amon can thereby uniquely located.

AML is a Bayesian approach which infers the energy of *any* query compound, no matter its size or composition, based on a linear combination of properly weighted quantum chemistry results for its constituting building blocks. The electronic locality assumption (“nearsightedness”) [45] underpinning the AML approach, is exploited to systematically converge the effective energy contributions coming from the various fragments in a molecule. AML enables instantaneous energy predictions with unprecedented predictive power, on par with experimental uncertainties: We have demonstrated the versatility and robustness of AML for numerical error convergence results for predicted energies of two dozen large

biomolecules with up to 96 heavy atoms, eleven thousand organic molecules with nine heavy atoms, non-covalently bound systems consisting of water clusters and Watson-Crick DNA base pairs, as well as doped hexagonal BN sheets and bulk silicon.

Using amons with at most seven heavy atoms, chemical accuracy (~ 1 kcal/mol) is reached for most covalently bound systems. Since identical amons are common to diverse chemistries of arbitrary query molecules, our results suggest that an amon training set of very finite size and consisting of small to medium sized molecules will suffice to generate accurate and efficient AML models applicable to a practically infinite number of chemical systems. Therefore, we think it evident that high-level reference energies, such as post-Hartree-Fock or Quantum Monte Carlo methods, are no longer prohibitive for future AML models, effectively promising to finally sidestep the various issues which plague many of the common DFT approximations [46]. Future work will deal with developments of more sophisticated amon selection procedures to also account for distorted or reactive structures, predictions of other extensive properties, and extensions of the amon pool to include further chemical elements, as well as open-shell, charged and electronically excited species.

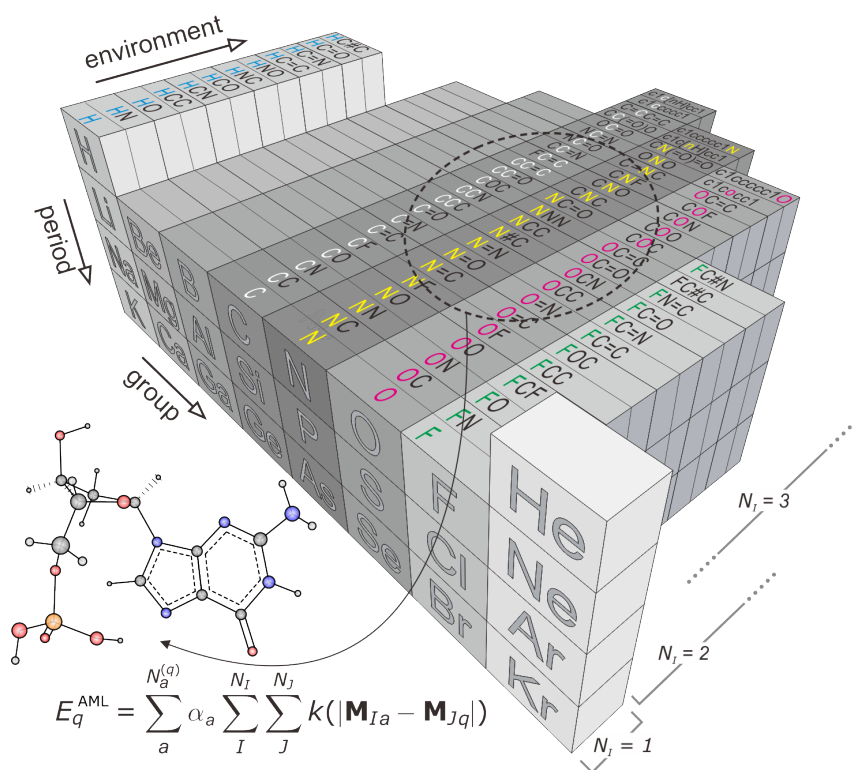


Figure 1. **Illustration of the “amons” of chemistry** as a compositional extension of the periodic table (for clarity only shown for main-group elements C, H, O, N, and F) in terms of SMILES strings arranged in increasing number of surrounding elements, and covering typical chemical environments. Within our amon machine learning approach, the energy of a query compound E_q (exemplary guanine nucleotide on display) is expanded in N_a amons, the double summation being weighted by kernel ridge regression coefficients $\{\alpha_a\}$, and quantifying the similarity k between all respective N_J and N_I atoms in query and amon molecule \mathbf{M}_q and \mathbf{M}_a .

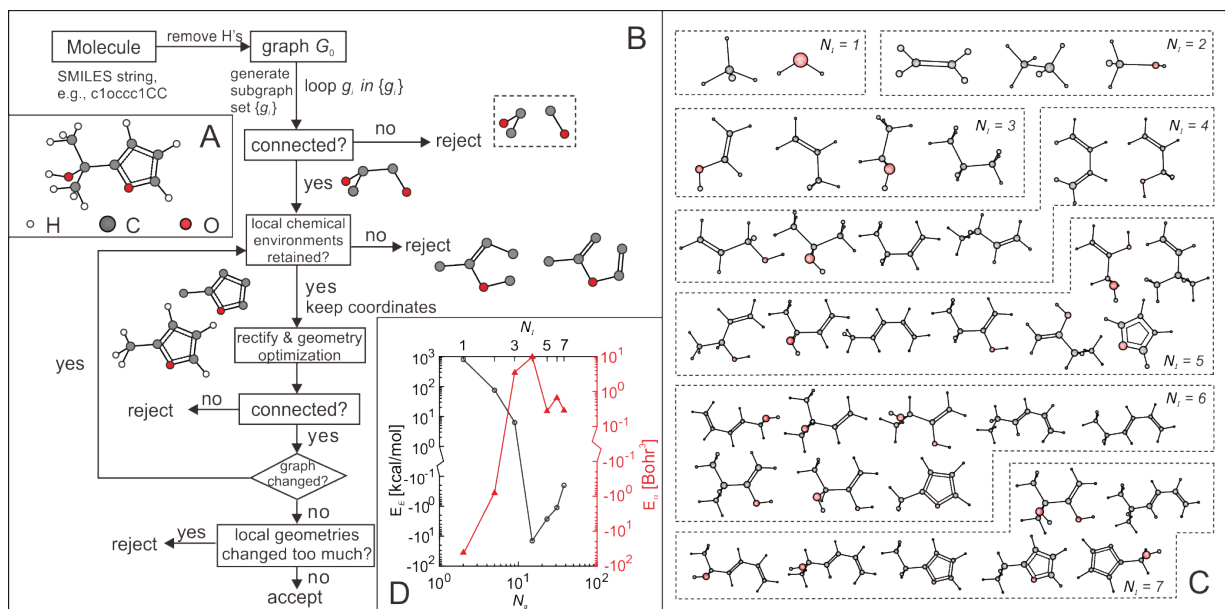


Figure 2. **Amon selection:** (A) Illustration of algorithm, exemplified for prediction of 2-(furan-2-yl)propan-2-ol; (B) Flow-chart for graph-based selection of amons; (C) Selected amons for query molecule; (D) Signed error E of predicted total energy (black) and isotropic static polarizability (red) as a function of number of amons in training set (N_a) or number of heavy atoms per amon (N_I , not counting hydrogens), respectively.

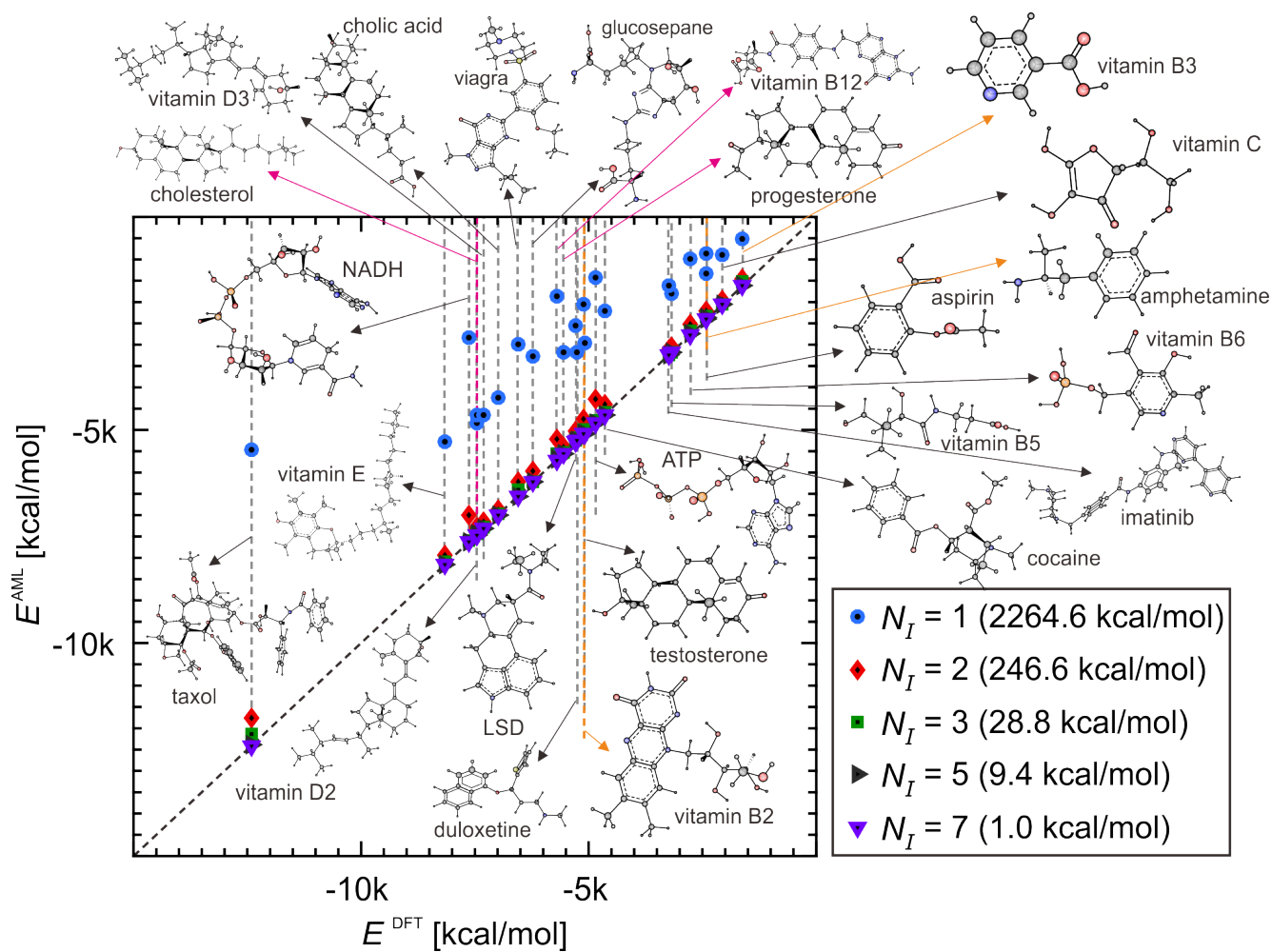


Figure 3. **Applicability of AML**, demonstrated by systematic improvement of predicted atomization energies (E) for two dozen important biomolecules using increasingly larger amons. The inset specifies the maximal number of heavy atoms (N_I , not counting hydrogens) per amon, as well as resulting MAE. Chemical, DFT, and bond-counting accuracy is roughly reached for amons with 7, 5 and 3 heavy atoms, respectively. All amons used are specified in supplementary materials.

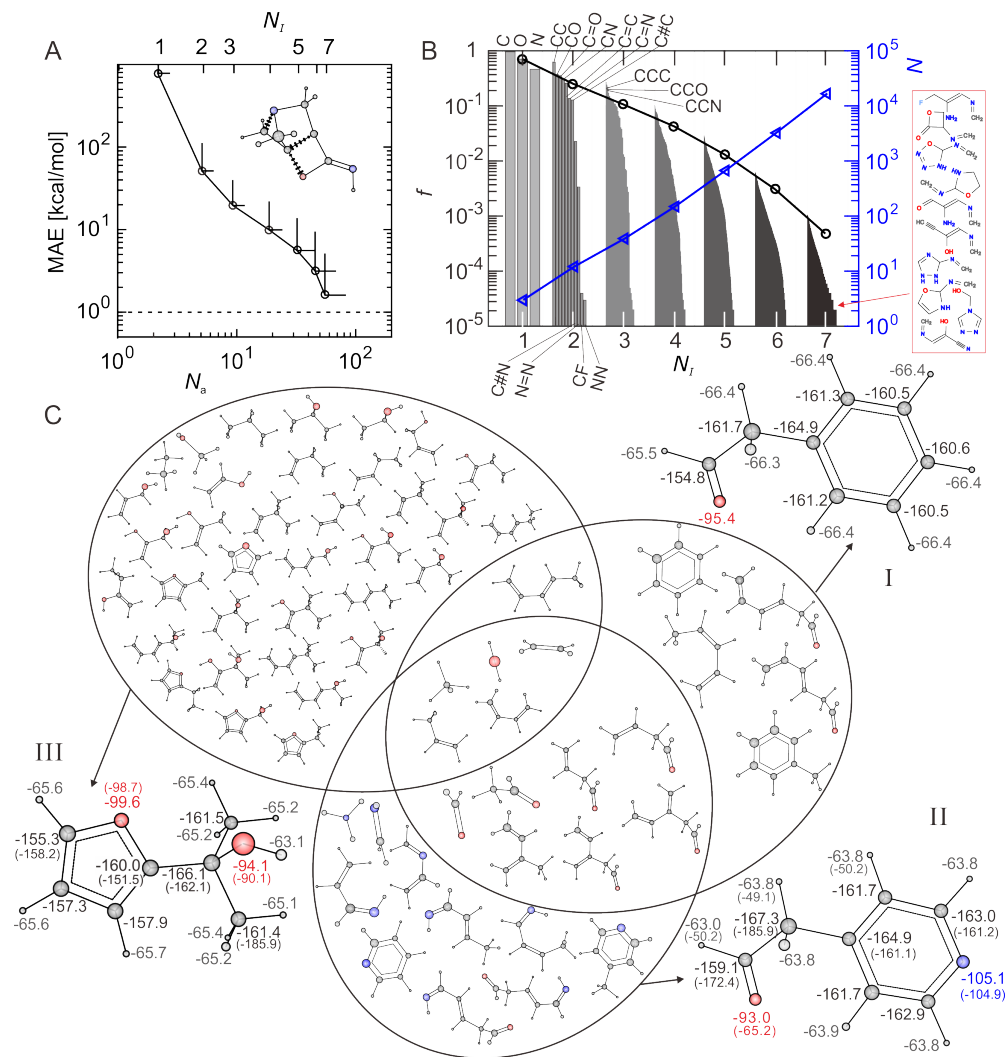


Figure 4. **The amons of organic chemistry:** (A) Mean absolute prediction error (circles) of total potential energy of eleven thousand organic molecules (with $N_I = 9$ from QM9 [34]) as a function of number of heavy atoms per amon (N_I , not counting hydrogens) or amons (N_a) in training set. Standard deviations with respect to error and N_a are also shown. The inset shows a typical outlier with high strain. (B) Left axis: Frequency of amons ($f = \text{number of occurrence}/\text{number of query molecules}$) in descending order; right axis: Number of query molecules N , both as a function of N_I of amons. Insets specify the most and least frequent amons. (C) amons for 2-phenylacetaldehyde (I), 2-(furan-2-yl)propan-2-ol (II) and 2-(pyridin-4-yl)acetaldehyde (III). Overlapping regions correspond to shared amons. Numbers indicate atomic energy contributions to atomization energy, regressed by AML and by Morse-potential (in brackets) for those atoms where meaningful.

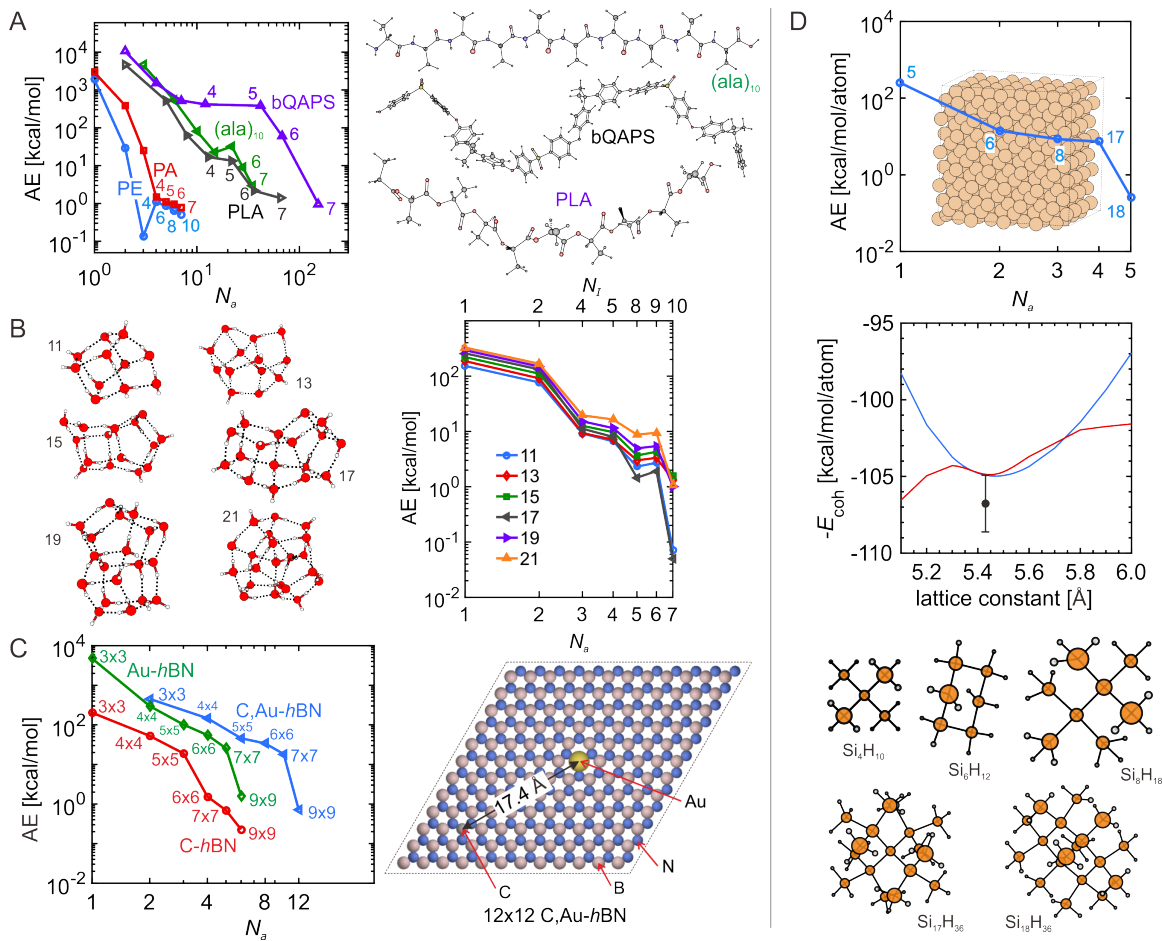


Figure 5. **Scalability of the AML model**, illustrated by learning curves for (A) 6 polymers, including polyethylene (PE, with 28 monomers), polyacetylene (PA, with 15 monomers), alanine peptide ((ala)₁₀), polylactic acid (PLA, with 10 monomers) and the backbone of quaternary ammonium polysulphate (bQAPS, with 3 monomers); (B) 6 water clusters with number of water molecules being 11, 13, 15, 17, 19, and 21; (C) 2-D hexagonal BN sheets with one B atom replaced by gold (Au-hBN), or carbon (C-hBN), or two B atoms replaced by gold and carbon (Au,C-hBN). Absolute errors are shown for per unit cell; (D) bulk silicon, for which also shown in the figure are predicted and DFT cohesive energies versus lattice constants (middle panel, where the black solid dot and vertical line represent experimental values [47, 48] and uncertainty of E_{coh} , respectively), as well as the amons (bottom panel, i.e., Si clusters saturated by hydrogens). Numbers of heavy atoms in amons (N_l) employed are specified in all learning curves. All amons not shown here are specified in supplementary material.

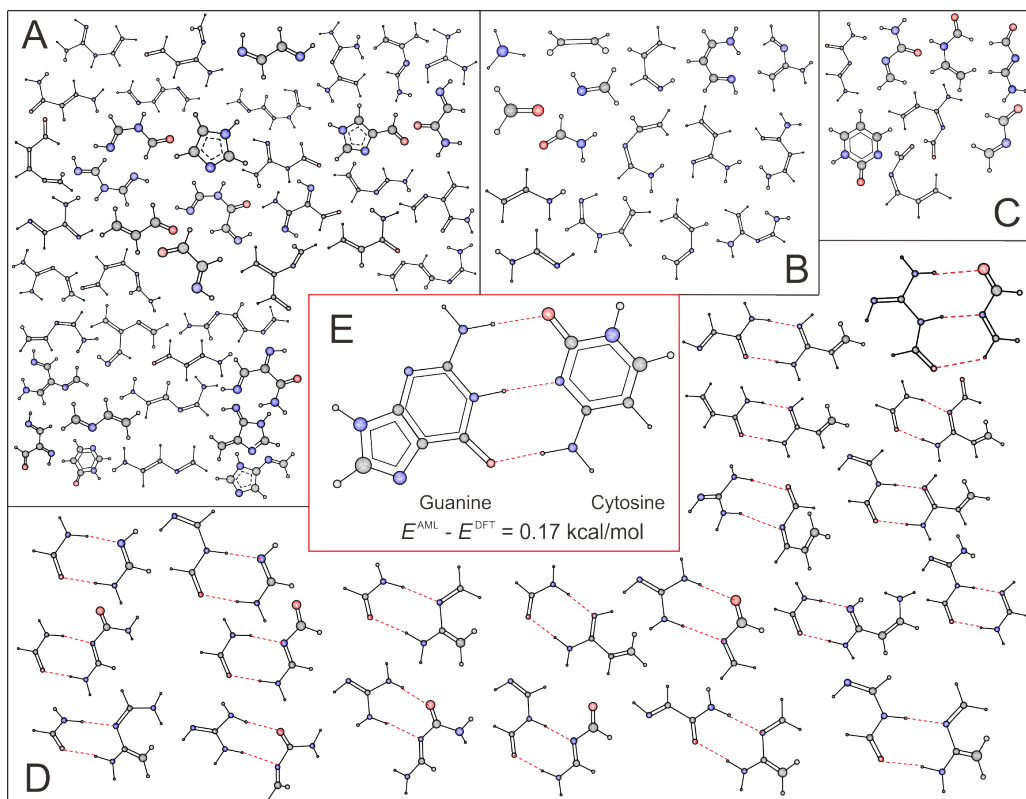


Figure 6. **The amoms of DNA**, illustrated for Watson-Crick base-pair GC (E). (A) amoms of DNA base Guanine; (B) amoms shared by Cytosine and Guanine; (C) amoms of Cytosine; (D) amoms of Watson-Crick bonding pattern, all containing H-bonds. Trained on these amoms, AML underestimates the DFT energy by 0.17 kcal/mol.

METHODS

For each atom J in query molecule q the model sums over amons with chemically similar atomic environments. More specifically, we rely on a kernel ridge regression model which approximates the energy difference between the truth and a baseline energy consisting of the sum of dressed atom energies (ε_0^J) which vary only among different elements and are obtained through fitting to the amons. For finite training set N_a ,

$$E_q^{\text{true}} \approx \sum_J \varepsilon_0^J + E_q^{\text{AML}}$$

where E_q^{AML} is the ML model specified in Figure 1, \mathbf{M}_{Ia} and \mathbf{M}_{Jq} are the respective representations of atoms I and J in molecules a and q . The selection of N_a fragments is done independently for each query, and from scratch, following the algorithm shown in Figure 2B and in the Supplementary Materials. Regression weights $\{\alpha_a\}$ are generated “on-the-fly” through inversion of the covariance matrix $K_{ha} = \sum_{JL} k(|\mathbf{M}_{Jh} - \mathbf{M}_{La}|)$ between all training amons a and h . We use the Euclidean norm in Gaussian kernels with heuristically determined amon-dependent widths. The atomic environment of atom I is represented by the atomic SLATM (spectrum of London (two-body) and Axilrod-Teller-Muto (three-body) potentials). We refer to the supplementary materials for more details.

Selection of conformational amons for any query molecule is carried out according to the flowchart in Figure 2. A molecule is a graph (G) defined by a set of vertices and edges $\{V, E\}$ with different weights for V and E (which represent different atom/bond types). From this set we select a subset $\{V_1, E_1\}$ (note that the 3D coordinates of each vertex is kept the same as the corresponding part in parent molecule, i.e., the query molecule) and proceed only if the new set is monomorphic. The monomorphic fragments are relaxed after saturation with hydrogens. The amon is expelled if the geometry relaxation leads to major atomic rearrangements which does not retain the chemical environment of the parent graph. This procedure is repeated until all subgraphs in G have been exhausted.

SUPPLEMENTARY MATERIAL

More technical details as well as coordinates and energies are provided in the supplementary materials.

AUTHOR CONTRIBUTIONS

All authors contributed extensively to the work presented in this paper.

ACKNOWLEDGEMENTS

D. Bakowies is acknowledged for helpful discussions. M. Caillard is acknowledged for the VR video of the 1k most frequent amons in QM9. O.A.v.L. acknowledges funding from the Swiss National Science foundation (No. PP00P2_138932 and 407540_167186 NFP 75 Big Data). This research was partly supported by the NCCR MARVEL, funded by the Swiss National Science Foundation. Calculations were performed at sciCORE (<http://scicore.unibas.ch/>) scientific computing core facility at University of Basel.

AUTHOR INFORMATION

Reprints and permissions information is available at www.nature.com/reprints. The authors declare no competing financial interests. Readers are welcome to comment on the online version of the paper. Correspondence should be addressed to O.A.v.L. (anatole.vonlilienfeld@unibas.ch). Requests for materials should be addressed to B.H. (bing.huang@unibas.ch).

* anatole.vonlilienfeld@unibas.ch

- [1] R. P. Feynman, R. B. Leighton, and M. Sands, *The Feynman lectures on physics. Vol. 1* (Addison-Wesley, 1963).
- [2] R. M. Martin, *Electronic structure: basic theory and practical methods* (Cambridge university press, 2004).
- [3] J. B. Reece, L. A. Urry, M. L. Cain, S. A. Wasserman, P. V. Minorsky, R. B. Jackson, *et al.*, *Campbell biology* (Pearson Boston, 2011).
- [4] P. Kirkpatrick and C. Ellis, *Nature* **432**, 823 (2004).
- [5] P. Hohenberg and W. Kohn, *Phys. Rev.* **136**, B864 (1964).
- [6] K. Burke, *J. Chem. Phys.* **136**, 150901 (2012).
- [7] J. Behler and M. Parrinello, *Phys. Rev. Lett.* **98**, 146401 (2007).
- [8] M. Schmidt and H. Lipson, *Science* **324**, 81 (2009).
- [9] A. P. Bartók, M. C. Payne, R. Kondor, and G. Csányi, *Phys. Rev. Lett.* **104**, 136403 (2010).
- [10] M. Rupp, A. Tkatchenko, K.-R. Müller, and O. A. von Lilienfeld, *Phys. Rev. Lett.* **108**, 058301 (2012).
- [11] A. Rodriguez and A. Laio, *Science* **344**, 1492 (2014).
- [12] E. O. Pyzer-Knapp, K. Li, and A. Aspuru-Guzik, *Adv. Fun. Mat.* **25**, 6495 (2015).
- [13] F. A. Faber, A. Lindmaa, O. A. von Lilienfeld, and R. Armiento, *Phys. Rev. Lett.* **117**, 135502 (2016).
- [14] P. Raccuglia, K. C. Elbert, P. D. F. Adler, C. Falk, M. B. Wenny, A. Mollo, M. Zeller, S. A. Friedler, J. Schrier, and A. J. Norquist, *Nature* **533**, 73 (2016).
- [15] C. R. Collins, G. J. Gordon, O. A. von Lilienfeld, and D. J. Yaron, <https://arxiv.org/abs/1701.06649> (2017).
- [16] A. Mannodi-Kanakkithodi, G. Pilania, T. D. Huan, T. Lookman, and R. Ramprasad, *Sci. Rep.* **6**, 20952 (2016).

- [17] G. Carleo and M. Troyer, *Science* **355**, 602 (2017).
- [18] K. T. Schütt, F. Arbabzadah, S. Chmiela, K. R. Müller, and A. Tkatchenko, *Nat. Commun.* **8**, 13890 (2017).
- [19] S. Chmiela, A. Tkatchenko, H. E. Sauceda, I. Poltavsky, K. T. Schütt, and K.-R. Müller, *Sci. Adv.* **3**, e1603015 (2017).
- [20] F. A. Faber, L. Hutchison, B. Huang, J. Gilmer, S. S. Schoenholz, G. E. Dahl, O. Vinyals, S. Kearnes, P. F. Riley, and O. A. von Lilienfeld, <https://arxiv.org/abs/1702.05532> (2017).
- [21] K. Kitaura, E. Ikeo, T. Asada, T. Nakano, and M. Uebayasi, *Chem. Phys. Lett.* **313**, 701 (1999).
- [22] S. Saebo and P. Pulay, *Annu. Rev. Phys. Chem.* **44**, 213 (1993).
- [23] M. Schütz, G. Hetzer, and H.-J. Werner, *J. Chem. Phys.* **111**, 5691 (1999).
- [24] W. Yang, *Phys. Rev. Lett.* **66**, 1438 (1991).
- [25] M. Gillan, D. Bowler, A. Torralba, and T. Miyazaki, *Comput. Phys. Comm.* **177**, 14 (2007).
- [26] R. M. Richard, K. U. Lao, and J. M. Herbert, *Acc. Chem. Res.* **47**, 2828 (2014).
- [27] K. Raghavachari and A. Saha, *Chem. Rev.* **115**, 5643 (2015).
- [28] W. J. Hehre, R. Ditchfield, L. Radom, and J. A. Pople, *J. Am. Chem. Soc.* **92**, 4796 (1970).
- [29] T. A. Halgren, *J. Comp. Chem.* **20**, 720 (1999).
- [30] R. Ramakrishnan, P. Dral, M. Rupp, and O. A. von Lilienfeld, *J. Chem. Theory Comput.* **11**, 2087 (2015).
- [31] W. Koch and M. C. Holthausen, *A Chemist's Guide to Density Functional Theory* (Wiley-VCH, 2002).
- [32] S. E. Wheeler, *WIREs Comput. Mol. Sci.* **2**, 204 (2012).
- [33] L. Ruddigkeit, R. van Deursen, L. C. Blum, and J.-L. Reymond, *J. Chem. Inf. Model.* **52**, 2864 (2012).
- [34] R. Ramakrishnan, P. Dral, M. Rupp, and O. A. von Lilienfeld, *Sci. Data* **1**, 140022 (2014).
- [35] O. A. von Lilienfeld, *Int. J. Quantum Chem.* **113**, 1676 (2013).
- [36] R. F. Bader, *Atoms in molecules* (Wiley Online Library, 1990).
- [37] B. Huang and O. A. von Lilienfeld, *J. Chem. Phys.* **145**, 161102 (2016).
- [38] S. Lu, J. Pan, A. Huang, L. Zhuang, and J. Lu, *Proc. Natl. Acad. Sci. USA* **105**, 20611 (2008).
- [39] T. James, D. J. Wales, and J. Hernández-Rojas, *Chem. Phys. Lett.* **415**, 302 (2005).
- [40] K. Mao, L. Li, W. Zhang, Y. Pei, X. C. Zeng, X. Wu, and J. Yang, *Sci. Rep.* **4**, 5441 (2014).
- [41] K.-R. Müller, M. Finke, N. Murata, K. Schulten, and S. Amari, *Neural Comput.* **8**, 1085 (1996).
- [42] C. Perlich, in *Encyclopedia of Machine Learning* (Springer, 2011) pp. 577–580.
- [43] N. J. Browning, R. Ramakrishnan, O. A. von Lilienfeld, and U. Roethlisberger, *J. Phys. Chem. Lett.* **8**, 1351 (2017).
- [44] A. Pérez, M. E. Tuckerman, H. P. Hjalmarson, and O. A. von Lilienfeld, *J. Am. Chem. Soc.* **132**, 11510 (2010).
- [45] E. Prodan and W. Kohn, *Proc. Natl. Acad. Sci. USA* **102**, 11635 (2005).
- [46] M. G. Medvedev, I. S. Bushmarinov, J. Sun, J. P. Perdew, and K. A. Lyssenko, *Science* **355**, 49 (2017).
- [47] Y. Okada and Y. Tokumaru, *J. Appl. Phys.* **56**, 314 (1984).
- [48] B. Farid and R. Godby, *Phys. Rev. B* **43**, 14248 (1991).